

Novel Compressible Adaptive Spectral Mixture Kernels for Gaussian Processes with Sparse Time and Phase Delay Structures

Kai Chen, Yijue Dai, Feng Yin *Senior Member*, Elena Marchiori, and Sergios Theodoridis *IEEE Life Fellow*

Abstract—Spectral mixture (SM) kernels comprise a powerful class of kernels for Gaussian processes (GPs) capable of discovering structurally complex patterns and modeling negative covariances. Being a linear superposition of quasi-periodical kernel components, the state-of-the-art SM kernel does not consider component compression and dependency structures between components. In this paper, we investigate the benefits of component compression and modeling of both time and phase delay structures between basis components in the SM kernel. By verifying the presence of dependencies between function components using Gaussian conditionals and posterior covariance, we first propose a new SM kernel variant with a time and phase delay dependency structure (SMD) and then provide a structure adaptation (SA) algorithm for the SMD. The SMD kernel is constructed in two steps: first, time delay and phase delay are incorporated into each basis component; next, cross-convolution between a basis component and the reversed complex conjugate of another basis component is performed, which yields a complex-valued and positive definite kernel incorporating dependency structures between basis components. The model compression and dependency sparsity of the SMD kernel can be obtained by using automatic pruning in SA. We perform a thorough comparative experimental analysis of the SMD on both synthetic and real-life datasets. The results corroborate the efficacy of the dependency structure and SA in the SMD.

Index Terms—Gaussian processes, spectral mixture, dependency structure, time and phase delay, structure adaptation.

I. INTRODUCTION

Gaussian processes (GPs) constitute an important class of Bayesian nonparametric models for machine learning [1]. A GP models an underlying system by applying a Gaussian prior to the underlying input-output modelling function and computes the posterior distribution over this function given the observations. This allows GPs to learn a function approximation well if a sufficient number of observations is accumulated. In addition, GPs can avoid overfitting in cases where only little evidence [2], [3] is available. A GP is able to model a large class of systems through the selection and design of the kernel function, which reflects the autocovariance structure of the

underlying function. However, similar to other kernel learning-based approaches, such as support vector machines (SVMs), the selection and design of covariance functions (i.e., called kernels) is almost the most important factor in GP applications because kernels determine the representation ability of GPs and the learned posterior distribution can be changed significantly by using different kernels.

For GPs, kernel selection is usually done subjectively, heavily depending on the expert knowledge and empirical analysis of data patterns. There are a handful of base kernels and their combinations that can be applied for diversified GP applications, such as received signal strength (RSS) radio map modeling [4] and wireless traffic prediction [5], [6]. To minimize the need for human intervention, automatic [7], [8], [9] and optimal kernel design [10] is in high demand and has become popular for GPs. Recently, [7] introduced an automatic and flexible kernel called a spectral mixture (SM) by modeling the power spectral density (SD) with a sum of Gaussians. The SM kernel is derived from the inverse Fourier transform (FT) of the corresponding SD functions. For many applications, GPs with SM kernels can efficiently discover latent patterns in datasets [7], [11], [12] and make predictions [13], [14]. Specifically, SM kernels have been successfully employed in various applications, such as medical time series prediction [15], Arctic coastal erosion forecasting [16], and urban environmental monitoring in sensor networks [17]. However, in a GP model the SM kernel cannot directly capture dependency structures between components because it involves only autoconvolution of its basis components [7].

In this paper, we prove that there are extensive dependency structures between SM components and then introduce a framework for extending SM kernels to include time and phase delay dependency structures between components of SM. More specifically, we design a complex-valued Gaussian SD that incorporates both time delay and phase delay in the frequency domain and transform it back to the time domain through the application of the inverse FT. Using cross-convolution between a basis component and the reversed complex conjugate of another component, we then construct a complex-valued, positive definite kernel that is able to capture dependency structures between SM components. In particular, a structure adaptation (SA) algorithm is proposed in the spectral mixture kernel with time and phase delay dependency (SMD) structure to perform interpretable hyper-parameter initialization, model compression, and dependency sparsening. Capturing time and phase delay dependency structures between components can be beneficial for modeling vast phenomena, such as monthly

Kai Chen, Yijue Dai, and Feng Yin (correspondence author) are with School of Science and Engineering (SSE), The Chinese University of Hong Kong, Shenzhen, and affiliated with Future Network of Intelligence Institute (FNii), The Chinese University of Hong Kong, Shenzhen 518172, China (e-mail: chenka@cuhk.edu.cn, yijuedai@link.cuhk.edu.cn, yinfeng@cuhk.edu.cn).

Elena Marchiori is with the Institute for Computing and Information Sciences, Radboud University, 6525 EC Nijmegen, The Netherlands (e-mail: elenam@cs.ru.nl).

Theodoridis Sergios is with Department of Informatics and Telecommunications, the National and Kapodistrian University of Athens, Athens, Greece (e-mail: stheodor@di.uoa.gr).

river flow extrapolation, where the moon and sun are primarily responsible for the rising and falling of river tidal flows. The SA algorithm can prevent the hyper-parameter space from expansion and retain valid dependency structures in the SMD.

The resulting novel SMD kernel contains a time and phase delay dependence term for each pair of components. To analyze the dependency structure between components captured by the proposed kernel, we introduce the so-called learned dependency measure (see Equation 20). The newly proposed SMD kernel can be regarded as the generalization of the original SM kernel; that is, by only considering autoconvolution of basis components and with zero time and phase delay, it reduces to the SM kernel. Preliminary results of this work have been presented in [18]. This paper includes multiple new contributions, such as the complex-valued Gaussian SD, four variants of dependency structure and their interpretations, and a structure adaptation algorithm with bootstrap-based hyper-parameter initialization, model compression, and dependency sparsification.

In short, our main contributions can be summarized as follows:

- A complex-valued Gaussian mixture model (GMM) modeling SDs is proposed by using the properties of the FT and incorporates both time delay and phase delay in the frequency domain.
- We propose a generalized variant of the SM kernel that incorporates time and phase delay dependency structures between components, demonstrates good interpretability of the dependency structures, and more importantly enriches the expressiveness of the original SM kernel.
- We introduce a useful and interpretable structure adaptation algorithm including bootstrap-based hyper-parameter initialization (BI), model compression, and dependency structure sparsification for the SMD.
- We present the compression ratio (CR), α_{CR} , and sparsity ratio (SR), α_{SR} , to evaluate the model compression and sparse dependency of the SMD. Comprehensive comparisons in terms of interpretability, fitting performance, generalization, and robustness are performed with various state-of-the-art kernels.

We comparatively evaluate the performance of the SMD on synthetic and multiple real-world datasets. The results indicate that the SMD is capable of modeling sparse dependence structures with substantially fewer components in the time series, and at the same time the SMD achieves performance comparable to or better than that of various other baselines (also in a multidimensional setting) with smaller uncertainty intervals compared to various other baselines.

The rest of this paper is organized as follows. Background on GPs and SM kernels and a summary of the related works are given in Section II and Section III, respectively. In Section IV, we present our motivation for modeling the dependency structure in the SM kernel. Section V introduces our SMD kernel, which has four variants of the dependency structure. Section VI describes the specialization of the SA algorithm for the SMD. Section VII describes the differences and similarities between the SMD and other kernels. Section VIII describes

experiments on synthetic and real-world datasets. Concluding remarks and future works are reported in Section IX.

II. BACKGROUND

In this section, we review GPs for machine learning and SM kernels.

A. Gaussian processes

In this paper, we mainly consider scalar, real-valued GPs. Given an observation pair $\{\mathbf{x}_i \in \mathbb{R}^P, y_i\}$ with P dimensional input, a GP can represent a function map $y = f(\mathbf{x}) + \epsilon$ to approximate an underlying system, where ϵ is the noise. From the function-space view, a GP [1], [3] defines a prior distribution over functions, completely specified by its first-order and second-order statistics, namely, the mean function $m(\mathbf{x})$ and the covariance function $k(\mathbf{x}, \mathbf{x}')$. In general, a GP is defined as follows:

$$f(\mathbf{x}) \sim \mathcal{GP}(m(\mathbf{x}), k(\mathbf{x}, \mathbf{x}')) \quad (1)$$

Without loss of generality, we take the mean function to be zero [3] since the learning ability of the GP can be fully guaranteed by the use of a flexible covariance function. In this paper, we use the terms covariance function, kernel, and kernel function interchangeably.

Given a selected covariance function $k(\mathbf{x}, \mathbf{x}')$ and a training set $\mathcal{D} = \{X, \mathbf{y}\}$, we can predict the mean $\hat{\mathbf{y}}^*$ and variances $\mathbb{V}[\mathbf{y}^*]$ (that is, its uncertainty) for the testing set X^* in a GP model by using the inferred posterior predictive distribution $p(\mathbf{y}^* | X^*, X, \mathbf{y}) \sim \mathcal{N}(\hat{\mathbf{y}}^*, \mathbb{V}[\mathbf{y}^*])$ with

$$\hat{\mathbf{y}}^* = K^{*\top} (K + \sigma_n^2 I)^{-1} \mathbf{y} \quad (2)$$

$$\mathbb{V}[\mathbf{y}^*] = K^{**} - K^{*\top} (K + \sigma_n^2 I)^{-1} K^* \quad (3)$$

where $K^{**} \triangleq K(X^*, X^*)$, $K^{*\top} \triangleq K(X^*, X)$, and σ_n^2 is the noise variance of ϵ with $\epsilon \sim \mathcal{N}(0, \sigma_n^2)$. In addition, the covariance function $k(\mathbf{x}, \mathbf{x}')$ has free hyper-parameters Θ determining the qualities of the GP, such as signal variance and length scale. The inference of GP is performed by minimizing the negative log-marginal likelihood (NLML, denoted by \mathcal{L}):

$$\mathcal{L} \triangleq -\log p(\mathbf{y} | X, \Theta) \quad (4)$$

where \mathcal{L} is obtained through marginalization over the latent function $f(X)$ [1], [3].

B. Spectral mixture kernels

The SM kernel [7] has been derived with the aid of Bochner's theorem [19], [20]. The essence of this theorem is that a complex-valued function k on \mathbb{R}^P is the covariance function of a weakly stationary mean square continuous complex-valued random process on \mathbb{R}^P if and only if it can be represented as

$$k(\boldsymbol{\tau}) = \int_{\mathbb{R}^P} e^{2\pi i \mathbf{s}^\top \boldsymbol{\tau}} d\psi(\mathbf{s}), \quad (5)$$

where ψ is a positive finite measure and i denotes the imaginary unit. If ψ has density $\hat{k}(\mathbf{s})$, then \hat{k} is called the SD or power spectrum of k . Moreover, k and \hat{k} constitute an FT pair; that is, $\hat{k}(\mathbf{s}) = \mathcal{F}_{\boldsymbol{\tau} \rightarrow \mathbf{s}}[k(\boldsymbol{\tau})](\mathbf{s})$ and $k(\boldsymbol{\tau}) = \mathcal{F}_{\mathbf{s} \rightarrow \boldsymbol{\tau}}^{-1}[\hat{k}(\mathbf{s})](\boldsymbol{\tau})$, where

the operators $\mathcal{F}_{\tau \rightarrow s}$ and $\mathcal{F}_{s \rightarrow \tau}^{-1}$ denote the FT and the inverse FT, respectively.

Originally, the SM kernel [7] was constructed by approximating the underlying SD as a mixture of Q Gaussians in the frequency domain, which can approximate any stationary kernel with a sufficient number of Gaussian components. Specifically, the i -th component of the SM kernel in the frequency domain has the form $\hat{k}_{SM,i}(\mathbf{s}) = (\mathcal{N}(\mathbf{s}; \boldsymbol{\mu}_i, \Sigma_i) + \mathcal{N}(-\mathbf{s}; \boldsymbol{\mu}_i, \Sigma_i))/2$ to force the symmetry property of SD. With the application of the inverse FT, the SM kernel in the time domain can be derived as:

$$\begin{aligned} k_{SM}(\boldsymbol{\tau}) &= \sum_{i=1}^Q w_i k_{SM,i}(\boldsymbol{\tau}) \\ &= \sum_{i=1}^Q w_i \exp(-2\pi^2 \boldsymbol{\tau}^\top \Sigma_i \boldsymbol{\tau}) \cos(2\pi \boldsymbol{\tau}^\top \boldsymbol{\mu}_i), \end{aligned} \quad (6)$$

where Q is the number of the SM components, $k_{SM,i}(\boldsymbol{\tau}) = \mathcal{F}_{s \rightarrow \tau}^{-1}[\hat{k}_{SM,i}(\mathbf{s})](\boldsymbol{\tau})$ is the i -th SM component, w_i , $\boldsymbol{\mu}_i = [\mu_{i,1}, \dots, \mu_{i,P}]$, and $\Sigma_i = \text{diag}([\sigma_{i,1}^2, \dots, \sigma_{i,P}^2])$ are the signal magnitude, center frequency, and frequency bandwidth parameters of the i -th SM component, respectively.

III. RELATED WORK

There is a rich literature on GPs related to covariance function design and analysis [3], [7], [8]. In this section, we mainly focus our attention on the family of SM kernels [7], [12], [9] and some new variants. More related SM extensions are surveyed in [11], [18]. Similar to the compositional form of the SM kernel, additive GPs [8], [21] implicitly sum over some one-dimensional base kernels to construct a flexible kernel representation. However, the existing additive GPs assume that function components specified by GPs with its kernel components are independent. Another SM extension called the spectral mixture product (SMP) kernel with $k_{SMP}(\boldsymbol{\tau}|\Theta) = \prod_{p=1}^P k_{SM}(\boldsymbol{\tau}_p|\Theta_p)$ for the purpose of modeling image data or, more broadly, spatial data is introduced in [12]. SMP is constructed via a product of several kernels build on the input dimensions. For SMP, the function components specified by GPs with their kernel components are mutually independent. A generalized SM kernel [22] has been derived to unify both the stationary and the non-stationary SMs but does not consider the dependency structure between its kernel components. Purely non-stationary extensions of the SM (NSM) kernel [11], [23] demonstrate compelling ability to represent input-dependent covariances between inputs. The NSM can be written as

$$\begin{aligned} k_{NSM}(x, x') &= \sum_{i=1}^Q w_i(x) w_i(x') k_{Gibbs,i}(x, x') \\ &\quad \times \cos(2\pi(\mu_i(x)x - \mu_i(x')x')) \end{aligned} \quad (7)$$

where x is a one-dimensional input, $k_{Gibbs,i}(x, x')$ is a non-stationary Gibbs kernel replacing the exponential part of the SM kernel, and $w_i(x_i)$ and $\mu_i(x_i)$ are the parameterized w_i and μ_i in the SM kernel, respectively. Similar to other existing kernels, the NSM kernel does not consider the dependency structure between its components.

On the other hand, a quantification of the dependency between function components in GPs using posterior covariance was proposed in [21]. However, no further investigation in modeling the dependency is presented [21]. Recently, an approach was proposed in [18] that encodes dependency structures between components of an SM kernel. In [18], the main challenges in modeling time and phase delays between SM components in GPs are still unsolved.

Other difficult issues for the use of the SM include hyper-parameter initialization, selection of the number of kernel components for structure discovery, and kernel compression. Explainable structure discovery and inference of the SM have been investigated in [9], [24]. In [9], another hyper-parameter efficient inference approach fixes $\boldsymbol{\mu}_i$ and Σ_i in the SM and allows only w_i to be optimizable, which could result in a sparse SM kernel. In [24], a Lévy process was introduced to automatically select the number of SM components, but the selection is not stable and easily encounters overfitting. However, the inference and optimization of the SMD in terms of hyper-parameter initialization, model pruning and dependency structure sparsity have not yet been studied.

IV. MOTIVATION

In the original SM kernel [7], all components are additive, which means that any function f drawn from a GP with the SM kernel k_{SM} , that is, $f \sim \mathcal{GP}(0, k_{SM})$, can be described as

$$f = \sum_{i=1}^Q f_i, \quad (8)$$

where function component $f_i \sim \mathcal{GP}(0, w_i k_{SM,i})$ (that is, each f_i is drawn from a GP with kernel $w_i k_{SM,i}$, the i -th component of the SM). To simplify our notations, in this section, we use \mathbf{f}_i and \mathbf{f}_i^* to denote the respective function values evaluated with the training inputs X and testing inputs X^* , respectively. Obviously, this form implies that these function components (f_i and f_j) are independent and that no dependency between them is modeled.

From the linear form in Eq. (8), the SM kernel does not take into account or analyze the dependencies between components. On the other hand, from subplots (b) and (e) in Fig. 1, the intersection between two SM components is significant in the frequency domain. In practice, two arbitrary Gaussians may intersect with each other in the frequency domain. The closer they are, the larger the overlap is. The intersection indicates the shared patterns between SM components, which motivates us to focus on the representation of the dependency structure between SM components at different frequencies.

A. Dependency structures between spectral mixture components

The additive form of the SM kernel assumes that the f_i values are *a priori* independent.

Remark 1: With the aid of Gaussian conditional identities, the conditional distribution of a GP-represented function \mathbf{f}_i^* conditioned on $\mathbf{f}_i + \mathbf{f}_j$ can be expressed as:

$$\mathbf{f}_i^* | \mathbf{f}_{i+j} \sim \mathcal{N}(K_i^{*\top} K_{i+j}^{-1} \mathbf{f}_{i+j}, K_i^{**} - K_i^{*\top} K_{i+j}^{-1} K_i^*) \quad (9)$$

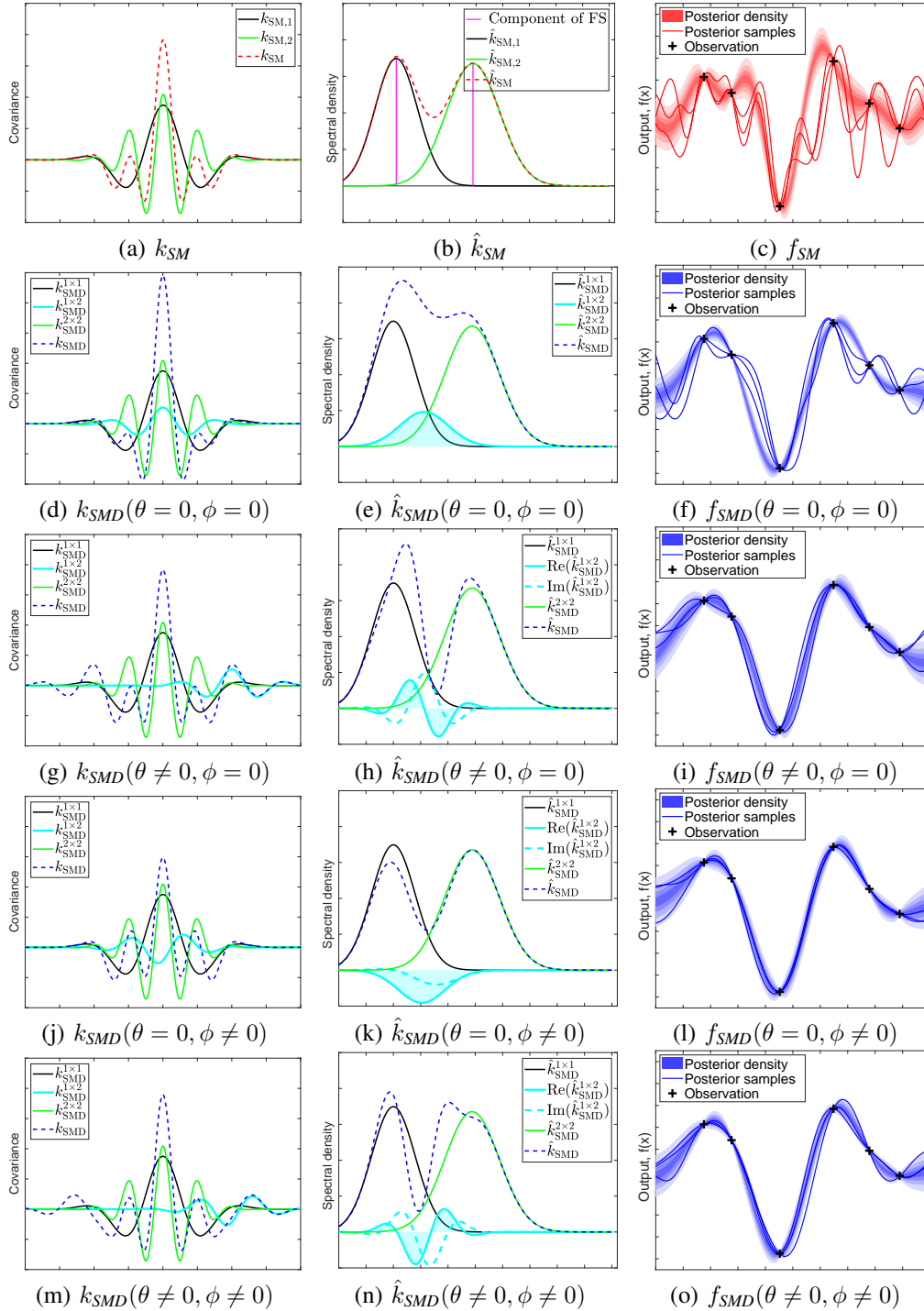


Fig. 1. Covariances, SDs, and posterior distributions based on GPs with the SM ($Q=2$) and SMD ($Q=2$) kernels conditioned on six observations. The first column: Covariances of SM (in red) and SMDs (in blue). The second column: components of Fourier series (FS) (in magenta, subplot (b)), SDs of SM (in red) and SMDs (in blue). The third column: posterior samples and distributions of SM (in red) and SMDs (in blue). The samples of all GP models were obtained using 200 equally spaced points. The legends of the first column, $k_{SMD}^{1 \times 1}$, $k_{SMD}^{2 \times 2}$, $k_{SMD}^{1 \times 2}$, and k_{SMD} , respectively, denote the covariances of the first component, the second component, the dependency structure between them, and the proposed SMD kernel. Note that the second column shows the corresponding SDs (denoted by hat) of the first column, where operators Re and Im denote the real and imaginary parts of an SD, respectively.

where $\mathbf{f}_{i+j} = \mathbf{f}_i + \mathbf{f}_j$ and $K_{i+j} = K_i + K_j$.

Readers can refer to [21] (Section 2.4.5) for the complete derivation of Eq. (9). Here, the Gaussian conditionals represent the model's posterior uncertainty regarding the different components of the signal, integrating over the possible configurations of the other components.

Remark 2: If there is no dependency between the function components \mathbf{f}_i and \mathbf{f}_j of SM, in general, we have $\mathbf{f}_i^* | \mathbf{f}_j = \mathbf{f}_i^* | \mathbf{f}_{i+j}$ (illustrated in Fig. 2).

Furthermore, computing the posterior covariance between two

functions, conditioned on their sum [21], leads to:

$$\text{Cov}(\mathbf{f}_i^*, \mathbf{f}_j^* | \mathbf{f}_{i+j}) = -K_i^{*\top} K_{i+j}^{-1} K_j^*. \quad (10)$$

To quantify the dependence between two arbitrary function components of SM, we normalize the posterior covariance as posterior correlation coefficient ρ_{ij} with range $[-1, 1]$:

$$\rho_{ij} = \frac{\text{Cov}(\mathbf{f}_i^*, \mathbf{f}_j^* | \mathbf{f}_{i+j})}{(\mathbb{V}(\mathbf{f}_i^* | \mathbf{f}_{i+j}) \mathbb{V}(\mathbf{f}_j^* | \mathbf{f}_{i+j}))^{1/2}}. \quad (11)$$

ρ_{ij} can be seen as an indicator of the dependence between the function components i and j of the SM. Note that there is no dependence if $\rho_{ij} = 0$; otherwise, they are dependent.

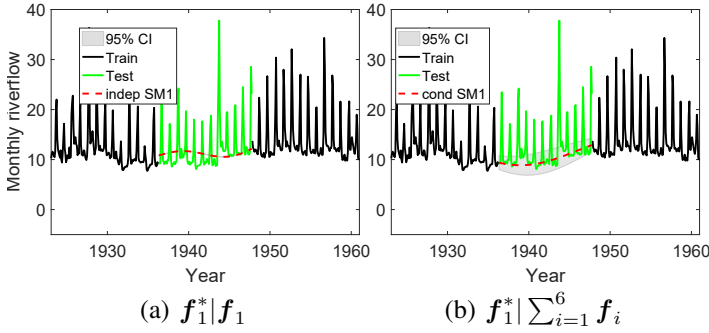


Fig. 2. Illustration of the conditional dependency ($\mathbf{f}_i^* | \mathbf{f}_i \neq \mathbf{f}_i^* | \mathbf{f}_{i+j}$) in a GP model using the SM kernel. (a) Prediction of $\mathbf{f}_i^* | \mathbf{f}_i$; (b) Prediction of $\mathbf{f}_i^* | \sum_{i=1}^6 \mathbf{f}_i$.

B. An illustration of the dependencies

We consider the monthly river flow dataset and the experimental settings described in Section VIII-D to illustrate the benefits of modeling the posterior covariance between function components. Specifically, we 1) train a GP using an SM kernel with $Q = 6$ components; 2) compute \mathbf{f}_i^* for $i = 1, \dots, Q$; 3) compute predictions using the (sum of) \mathbf{f}_i^* values conditioned on the sum of the \mathbf{f}_i values (see Eq. (9)): (a) $\mathbf{f}_i^* | \mathbf{f}_i$, and (b) $\mathbf{f}_i^* | \sum_{j=1}^Q \mathbf{f}_j$. For all plots in this section, the training data, the testing data, the predictions, and the predictive confidence intervals (CIs) are in black, green, dashed red, and gray, respectively.

From Fig. 2, the prediction of the $\mathbf{f}_1^* | \mathbf{f}_1$ in subplot (a) and the prediction of the $\mathbf{f}_1^* | \sum_{i=1}^6 \mathbf{f}_i$ in subplot (b) present quite different trends and CIs. The trend in subplot (a) demonstrates a quasiperiodic pattern with a very small and impractical CI. However, in subplot (b), we can see a linear rising trend with a larger CI. This difference results from the posterior covariance (see Eq. (9) and Eq. (10)). The differences in terms of uncertainty and pattern between subplots (a) and (b) indicate the corresponding differences between $\mathbf{f}_i^* | \mathbf{f}_i$ and $\mathbf{f}_i^* | \mathbf{f}_{i+j}$. This clearly confirms that $\mathbf{f}_i^* | \mathbf{f}_i \neq \mathbf{f}_i^* | \mathbf{f}_{i+j}$ and that there are dependencies between the function components of GPs using the SM kernel.

V. SPECTRAL MIXTURE KERNEL WITH TIME AND PHASE DELAYS

In this section, we propose for the first time an extended SM kernel that incorporates both time and phase delay. First, in

Section V-A, both time delay and phase delay are incorporated into each basis kernel component of the SM. Then, an SMD cross-component term is constructed by performing cross-convolution between a basis component and the reversed complex conjugate of another basis component (in Section V-B). Finally, the SMD cross-component terms are used to construct a complex-valued and positive definite kernel to represent the dependency structure between basis components (in Section V-C).

A. Complex-valued Gaussian spectral density

In signal processing, for a signal of an underlying process, time delay differences between signal frequency components characterize temporal relation between them and influence the shape of the signal. Furthermore, due to the nature of FT, a signal in the frequency domain always has a complex representation with magnitude (real) and phase (imaginary) parts. It can be of interest to know not only the magnitude but also the phase of the SD. The phase difference is useful for understanding the phenomenon of interference (dependency structure) between components of a physical process. However, the dependency structure investigated in [18] only paints a picture of magnitude difference between the SM components. Thus, we introduce time and phase delays to the SD of SM components to enrich its representation power.

As is known from classic signal processing, shifting a signal in the time domain is equivalent to multiplying a complex exponential in the frequency domain [25]. Concretely, for any time delay function $k_\theta(\tau) = k(\tau - \theta)$ with a time delay vector θ , its FT is $\hat{k}_\theta(s) = e^{-2\pi\theta s} \hat{k}(s)$, where $\hat{k}(s) = \mathcal{F}_{\tau \rightarrow s}[k(\tau)](s)$ [26]. Moreover, for any phase delay function $k_\phi(\tau)$ with phase delay vector ϕ , the FT of $k_\phi(\tau)$ in the frequency domain is $\hat{k}_\phi(s) = e^{-2\pi\phi s} \hat{k}(s)$.

Therefore, in the frequency domain, we can directly embed the time delay θ_i and phase delay ϕ_i into the i -th Gaussian component $\hat{k}_{SM,i}(s)$ of the SM kernel, yielding the following complex-valued function, which we call the *time and phase delay SD* function:

$$\hat{k}_{SMD,i}(s) = w_i \varphi_{SM,i}(s) e^{-2\pi i(\theta_i s + \phi_i)} \quad (12)$$

where $\varphi_{SM,i}(s) = \mathcal{N}(s; \boldsymbol{\mu}_i, \Sigma_i)$.

B. Convolution of the time and phase delay components

A stationary covariance function $k(\mathbf{x}, \mathbf{x}')$ can be represented in convolution form on \mathbb{R}^P , as in [27], [28], as follows:

$$k(\mathbf{x}, \mathbf{x}') \triangleq \int_{\mathbb{R}^P} g(\mathbf{u}) g(\boldsymbol{\tau} - \mathbf{u}) d\mathbf{u} = (g * g)(\boldsymbol{\tau}), \quad (13)$$

where $\boldsymbol{\tau} \triangleq \mathbf{x} - \mathbf{x}'$ and $*$ denotes the convolution operator. Since performing convolution in the time domain corresponds to performing multiplication in the frequency domain, for the SM kernel, we have the squared form of the i -th SM component as

$$\begin{aligned} w_i \hat{k}_{SM,i}(s) &= \mathcal{F}_{\tau \rightarrow s}[(g_{SM,i} * g_{SM,i})(\boldsymbol{\tau})](s) \\ &= (\hat{g}_{SM,i}(s))^2, \end{aligned} \quad (14)$$

where $\hat{g}_{SM,i}(\mathbf{s})$ is the basis function of the i -th Gaussian. In our setting, however, we want to model dependency structures between components. One possible approach is to use the cross correlation between the underlying functions $f_i \sim \mathcal{GP}(0, w_i k_{SM,i})$ and $f_j \sim \mathcal{GP}(0, w_j k_{SM,j})$, which is similar in nature to the convolution of two kernels $w_i k_{SM,i}$ and $w_j k_{SM,j}$, defined as

$$f_i \star f_j = \mathcal{F}_{s \rightarrow \tau}^{-1} [w_i \varphi_{SM,i}(\mathbf{s}) \cdot \overline{w_j \varphi_{SM,j}(\mathbf{s})}] (\tau) \quad (15)$$

where $\mathcal{F}_{s \rightarrow \tau}^{-1}$, \star , and $\overline{(\cdot)}$ denote the inverse FT, the cross-correlation operator, and the complex conjugate operator, respectively. However, if we use Eq. (15) to express dependencies, then we obtain a kernel that is the inverse FT of the squared Gaussian $w_i^2 \varphi_{SM,i}^2(\mathbf{s})$ when $i = j$. This is different from the SM kernel. To ensure the compatibility between the dependency structure and SM component for $i = j$, we therefore consider the cross correlation between the *basis components* $g_{SM,i}$ of the i -th and the j -th SM components, where $g_{SM,i}(\tau) = \mathcal{F}_{s \rightarrow \tau}^{-1} [\hat{g}_{SM,i}(\mathbf{s})] (\tau)$.

Particularly, considering the time and phase delay SD function in Eq. (12) and applying the squared form in Eq. (14), we have the time and phase delay basis function of the SD, $\hat{k}_{SMD,i}(\mathbf{s}) = \sqrt{\hat{k}_{SMD,i}(\mathbf{s})}$. Now, for the purpose of expressing the dependency structure in the presence of the time and phase delay, we employ the basis function $\hat{g}_{SMD,i}(\mathbf{s})$ and define the SD of the dependency structure as

$$\begin{aligned} \hat{k}_{SMD}^{i \times j}(\mathbf{s}) &= \hat{g}_{SMD,i}(\mathbf{s}) \cdot \overline{\hat{g}_{SMD,j}(\mathbf{s})} \\ &= w_{ij} a_{ij} \underbrace{\mathcal{N}(\mathbf{s}; \boldsymbol{\mu}_{ij}, \Sigma_{ij})}_{\text{cross Gaussian SD}} \underbrace{\exp(-\pi i(\boldsymbol{\theta}_{ij} \mathbf{s} + \phi_{ij}))}_{\text{cross time and phase delay}} \end{aligned} \quad (16)$$

with the following parameters:

- cross weight: $w_{ij} = \sqrt{w_i w_j}$,
- cross amplitude: $a_{ij} = |4\pi^2 \Sigma_i \Sigma_j|^{-\frac{1}{4}} \mathcal{N}(\boldsymbol{\mu}_i; \boldsymbol{\mu}_j, \frac{\Sigma_i + \Sigma_j}{2})$,
- cross mean: $\boldsymbol{\mu}_{ij} = \frac{\Sigma_i \boldsymbol{\mu}_j + \Sigma_j \boldsymbol{\mu}_i}{\Sigma_i + \Sigma_j}$,
- cross covariance: $\Sigma_{ij} = \frac{2\Sigma_i \Sigma_j}{\Sigma_i + \Sigma_j}$,
- cross time delay: $\boldsymbol{\theta}_{ij} = \boldsymbol{\theta}_i - \boldsymbol{\theta}_j$,
- cross phase delay: $\phi_{ij} = \phi_i - \phi_j$.

Parameters $\boldsymbol{\mu}_{ij}$ and Σ_{ij} can be interpreted as the inverse period and inverse length scale of the component $k_{SMD}^{i \times j}(\tau) = \mathcal{F}_{s \rightarrow \tau}^{-1} [\hat{k}_{SMD}^{i \times j}(\mathbf{s})] (\tau)$. The cross amplitude a_{ij} is a normalization constant that depends on the difference between components i and j rather than \mathbf{s} . However, without time and phase delays, in the frequency domain, the SD term can be defined as follows: $\hat{k}_{SMD,\theta=0,\phi=0}^{i \times j}(\mathbf{s}) \triangleq \hat{g}_{SM,i}(\mathbf{s}) \cdot \overline{\hat{g}_{SM,j}(\mathbf{s})}$.

The kernel corresponding to this SD has been investigated in [18].

Remark 3: According to Eq. (16), the denser the mixture of Gaussian components in the SM is, the similar the weight w_{ij} , frequency $\boldsymbol{\mu}_{ij}$, and scale Σ_{ij} of the components in the SM, and the greater the contribution made by the cross convolution in the SMD.

C. Spectral mixture with time and phase delay dependency structure

In light of the SM kernel, by applying the inverse FT, we can define an SMD component (a new term in the proposed SM kernel for representing the dependency structure between two function components) in the time domain as

$$\begin{aligned} k_{SMD}^{i \times j}(\tau) &= \mathcal{F}_{s \rightarrow \tau}^{-1} [\hat{g}_{SMD,i}(\mathbf{s}) \cdot \overline{\hat{g}_{SMD,j}(\mathbf{s})}] (\tau) \\ &= c_{ij} \exp(-2\pi^2 \boldsymbol{\tau}_\theta^\top \Sigma_{ij} \boldsymbol{\tau}_\theta) \exp(i 2\pi(\boldsymbol{\tau}_\theta^\top \boldsymbol{\mu}_{ij} - \frac{\phi_{ij}}{2})), \end{aligned} \quad (17)$$

where $\boldsymbol{\tau}_\theta \triangleq \boldsymbol{\tau} - \frac{\boldsymbol{\theta}_{ij}}{2}$ is the Euclidean distance with time delay and $c_{ij} = w_{ij} a_{ij}$ is the normalization term incorporating the cross weight and cross amplitude and does not depend on τ . Note that c_{ij} indicates the largest degree of the dependency structure between components i and j in the SMD.

For an SM kernel with Q components, we can obtain the corresponding dependency structures by considering the distributivity of the convolution operator and the symmetric properties of SD as follows:

$$\begin{aligned} k_{SMD}(\tau) &= \sum_{i=1}^Q \sum_{j=1}^Q c_{ij} \underbrace{\exp(-2\pi^2 \boldsymbol{\tau}_\theta^\top \Sigma_{ij} \boldsymbol{\tau}_\theta)}_{\text{exponential decay term}} \\ &\quad \times \underbrace{(\cos(2\pi(\boldsymbol{\tau}_\theta^\top \boldsymbol{\mu}_{ij} - \frac{\phi_{ij}}{2})))}_{\text{periodic term}}. \end{aligned} \quad (18)$$

To show that Eq. (18) is a valid kernel, we need to prove that it is positive semidefinite (PSD). This is equivalent to saying that its SD, $\hat{k}_{SMD}(\mathbf{s})$, is PSD as well [19], [20]. Here, given any finite set of non-zero vectors $[\mathbf{z}_1, \dots, \mathbf{z}_N]^\top \in \mathbb{C}^{N \times P}$ with complex entries, $\mathbf{s} \in \mathbb{R}^P$, we have $\sum_{n=1}^N |(\sum_{i=1}^Q \mathbf{z}_n \hat{g}_{SMD,i}(\mathbf{s}))|^2 \geq 0$.

Thus, the sum of SDs satisfies the positive definite requirement. Therefore, it follows that Eq. (18) is PSD. From this equation, we can see that the SMD kernel is a mixture of periodic terms weighted by squared exponential terms, similar to the original SM kernel. In contrast to the SM kernel, the SMD also includes a dependency term for each of the Q^2 pairs of components. If we do not consider the time and phase delay dependency structures between different components, the components of the dependency structures are based only on the cross convolution of ordinary basis components in the SM [18]. In this case, the SMD becomes

$$\begin{aligned} k_{SMD,\theta=0,\phi=0}(\tau) &= \sum_{i=1}^Q \sum_{j=1}^Q c_{ij} \exp(-2\pi^2 \boldsymbol{\tau}^\top \Sigma_{ij} \boldsymbol{\tau}) \\ &\quad \times \cos(2\pi \boldsymbol{\tau}^\top \boldsymbol{\mu}_{ij}). \end{aligned} \quad (19)$$

In the SMD, each (i, j) term in Eq. (18) with $i \neq j$, that is, $k_{SMD}^{i \times j}(\tau)$, represents the dependency between components i and j captured by our kernel. In total, for the SMD, there are Q^2 structures (shown as connections in subplot (b) in Fig. 6) with Q original components (shown as connections in subplot (a) in Fig. 6) similar to the SM plus $Q^2 - Q$ dependency

structures (shown as cross connections in subplot (b) in Fig. 6). In addition, we use its normalized form

$$\gamma_{ij}(\boldsymbol{\tau}) = \frac{k_{SMD}^{i \times j}(\boldsymbol{\tau})}{\sqrt{w_i k_{SM,i}(\boldsymbol{\tau}) w_j k_{SM,j}(\boldsymbol{\tau})}} \quad (20)$$

as a measure of dependency between components represented by the SMD kernel. Note that for $i = j$, we have $\gamma_{ij} = 1$ when $w_i k_{SM,i}(\boldsymbol{\tau}) > 0$ and $\gamma_{ij} = -1$ when $w_i k_{SM,i}(\boldsymbol{\tau}) < 0$. Therefore, for the plot of γ_{ij} , there are stripe textures in the diagonal position.

VI. STRUCTURE ADAPTATION FOR THE SPECTRAL MIXTURE WITH DEPENDENCY STRUCTURE

Algorithm 1: SA algorithm for SMD

Input : $\mathcal{D} = \{X, \mathbf{y}\}$, Q_{init} , σ_n^2 , T_{prune} , T_{opt} , M_{init} , $\mathcal{L}_{init} = \infty$.
Output : Q_{prune} , Q_{rest} , $\{\Theta, \sigma_n^2\}$.

- 1 **for** M_{init} iterations **do**
- 2 Initialize $\tilde{\Theta}_{init}$ with Q_{init} using **Algorithm 2**;
- 3 Obtain $\tilde{\Theta}_{temp}$ by inferring the GP model with k_{SMD} , Q_{init} , $\tilde{\Theta}_{init}$, σ_n^2 , and T_{prune} ;
- 4 Compute \mathcal{L}_{temp} of $\mathcal{GP}(0, k_{SMD})$ with $\tilde{\Theta}_{temp}$;
- 5 **if** $\mathcal{L}_{temp} < \mathcal{L}_{init}$ **then**
- 6 $\mathcal{L}_{init} = \mathcal{L}_{temp}$;
- 7 Let $\tilde{\Theta}_{prune} = \tilde{\Theta}_{init}$ for pruning;
- 8 Keep the inferred hyper-parameters of better initialization with $\tilde{\Theta}_{better} = \tilde{\Theta}_{temp}$;
- 9 **end**
- 10 **end**
- 11 $Q_{prune} = 0$;
- 12 **for** $i = 0; i \leq Q_{init}$ **do**
- 13 Obtain the i -th weight w_i from $\tilde{\Theta}_{better}$;
- 14 **if** $w_i < 1$ **then**
- 15 Remove the i -th component in SMD;
- 16 Remove $\{w_i, \boldsymbol{\mu}_i, \Sigma_i, \boldsymbol{\theta}_i, \phi_i\}$ in $\tilde{\Theta}_{prune}$;
- 17 $Q_{prune} = Q_{prune} + 1$;
- 18 **end**
- 19 **end**
- 20 The number of components remaining is $Q_{rest} = Q_{init} - Q_{prune}$;
- 21 Quantify the intensity of the dependency structures;
- 22 Remove the low intensity dependency structures with $c_{ij} < 1$ and obtain dependency sparsity with β_{ij} ;
- 23 Optimize the GP model with the sparse SMD kernel, $\tilde{\Theta}_{prune}$, Q_{rest} , σ_n^2 , and T_{opt} ;
- 24 Obtain $\{\Theta, \sigma_n^2\}$ from the optimized GP model.

The SM kernel has been known for its relatively large number of hyper-parameters (with size $3Q$) since publication in [7]; this perturbs the inference and learning of GPs with the SM kernel. Critically, there are several de facto inference and learning issues impeding the use of the SM kernel, such as hyper-parameter initialization and selection of the number of kernel components. The proposed SMD also inherits these issues. In addition, the dependency structures in SMD are dense (with

$Q^2 - Q$ dependency structures) and therefore introduce another problem of how to obtain sparsity for these structures. In this section, we propose a structure adaptation (SA) algorithm (see **Algorithm 1**) for the SMD to handle the above issues and to achieve efficient inference and interpretable structure discovery.

Concisely, the symbols and notations in the SA algorithm include the dataset, $\mathcal{D} = \{X, \mathbf{y}\}$; initial number of components, Q_{init} ; pruned number of components, Q_{prune} ; the number of components after pruning, Q_{rest} ; length of the run for pruning, T_{prune} ; length of the run for optimization, T_{opt} ; number of initialization attempts, M_{init} ; initial hyper-parameters, $\tilde{\Theta}_{init}$; temporary inferred hyper-parameters, $\tilde{\Theta}_{temp}$; inferred hyper-parameters of a better initialization, $\tilde{\Theta}_{better}$; the selected hyper-parameters for pruning, $\tilde{\Theta}_{prune}$; final inferred hyper-parameters, $\{\Theta, \sigma_n^2\}$; initial NLML, $\mathcal{L}_{init} = \infty$; and temporary NLML computed by using $\tilde{\Theta}_{temp}$, \mathcal{L}_{temp} .

In **Algorithm 1**, steps 1-10 perform M_{init} initializations using the proposed method shown in **Algorithm 2** and then compare the NLML values of M_{init} initializations to obtain a better initialization with the minimal NLML value. Based on the chosen better initialization, steps 11-20 prune the unimportant kernel components by determining their weights. Steps 21-22 facilitate the sparsity of the dependency structures by quantifying the intensity of the dependency structures and removing the weak dependency structures in the SMD.

Specifically, in SA, a novel hyper-parameter initialization using bootstrap can effectively improve initialization accuracy, which is shown in Section VI-A. In Section VI-B, an effective pruning method included in SA is shown that can automatically select the number of kernel components, avoid overfitting, and thus greatly reduce the hyper-parameter space. In Section VI-C, we show how the SA algorithm obtains sparsity in dependence structures.

A. Bootstrap-based hyper-parameter initialization

Algorithm 2: A BI algorithm

Input : $\mathcal{D} = \{X, \mathbf{y}\}$, Q_{init} , $B = 100$.
Output : $\tilde{\Theta}_{init}$.

- 1 Compute the empirical SD $S = \{\mathbf{s}_1, \dots, \mathbf{s}_n\}^\top$ using the Blackman window and FT;
- 2 Resample the bootstrap spectral samples $S^* = \{\mathbf{s}_1^*, \dots, \mathbf{s}_n^*\}^\top$ from S ;
- 3 Fit a GMM with Q_{init} components in S^* to obtain a bootstrap estimation $p(\tilde{\Theta}^* | \mathbf{s}^*)$ using Eq. (21);
- 4 Sort Q_{init} components with mean position $\boldsymbol{\mu}_i^*$ to keep the CI of each component;
- 5 Repeat steps 2-4 B times to obtain B estimations $p(\tilde{\Theta}_1^* | \mathbf{s}^*), p(\tilde{\Theta}_2^* | \mathbf{s}^*), \dots, p(\tilde{\Theta}_B^* | \mathbf{s}^*)$;
- 6 The bootstrap estimations of the hyper-parameters are approximated as $\tilde{\Theta}_{init} = \frac{1}{B} \sum_{i=1}^B \tilde{\Theta}_i^*$.

The learning of the SMD kernels is quite sensitive to the starting point of optimization in high-dimensional hyper-parameter space. A better initialization can help us more easily discover the underlying structure and fairly compare

the performance returned by different benchmark kernels. Informatively, the motivation of the SM kernel illuminates the interpretation of hyper-parameters in the frequency domain and the connection between the empirical SD and kernel. Therefore, sniffing the structure of the empirical SDs can alleviate the difficulty of hyper-parameter initialization. In the experiments described in the next section, the empirical SDs containing prior information extracted from training data are used to find better initialization values of hyper-parameters as recommended in [7], [23]. However, the empirical SDs are biased observations of the true underlying spectral structures. The empirical SDs contain much noise and fake peaks denoting spurious patterns. To filter out the noise and fake peaks, we employ the Blackman window function for the FT and bootstrap techniques [29], [30] to improve the estimation accuracy of the empirical SDs. Bootstrap is a general and widely applicable method for approximating a distribution of interest. We draw a large number of spectral samples (bootstrap samples S^*) using bootstrap with replacement from the empirical SDs. We then consider a Gaussian mixture model (GMM) fitting to the bootstrap samples S^* to obtain the Q centers of the Gaussian SDs.

$$p(\tilde{\Theta}|s^*) = \sum_{i=1}^Q \tilde{w}_i \mathcal{N}(s^*; \tilde{\mu}_i, \tilde{\Sigma}_i) \quad (21)$$

Finally, we propose a BI algorithm (shown in **Algorithm 2**) for the SMD. The bootstrap sampling times $B = 100$ is found to be sufficient for robust statistics estimation.

The estimation of the hyper-parameter obtained in **Algorithm 2** is used for initialization. An illustration of Algorithm 2 is shown in Fig. 3. For all kernels, we select the hyper-parameters with the lowest NLML over 10 initialization trials. The selected hyper-parameters are then used for GP optimization.

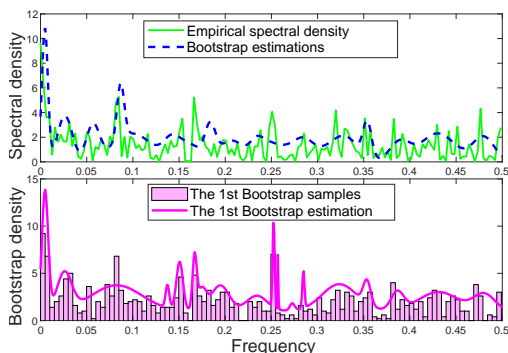


Fig. 3. Illustration of the BI algorithm using the monthly river flow dataset. Subplot in the first row: the empirical SD (in green line) and bootstrap estimation (in dashed blue line). Subplot in the second row: the 1st bootstrap samples (in magenta bar) and the corresponding estimation (in magenta line). Here, many small peaks in empirical SD are filtered in the bootstrap estimation.

B. Efficient hyper-parameter pruning for compressed spectral mixtures with dependency structures

In addition to the aforementioned hyper-parameter initialization, how to set the number of components is another tangible

issue of the SM and SMD. Specifically, for the SMD and SM, we have to specify the Q in advance and treat it as fixed during inference. However, Q cannot reflect the true number of underlying patterns contained in data, which could lead to overfitting if Q is large. This problem makes the SMD flawed and impractical for real-world applications. To adaptively select the number of components and gain efficient hyper-parameter pruning in SM and SMD, in this section, we first prune the less important components by revealing the weight of the components. Concretely, we consider the monthly river flow dataset and experimental settings described in Section VIII-D to demonstrate the learned importance of components in the SM kernel. Specifically, we train a GP using an SM kernel with $Q = 10$ components and show the details of all learned w_i in subplot (a) in Fig. 4. By analyzing all learned w_i , we find that the weights of these components ($i = \{1, 2, 3, 6, 8, 9\}$) are smaller than 1, which means that the corresponding amplitudes in the frequency domain are fairly small.

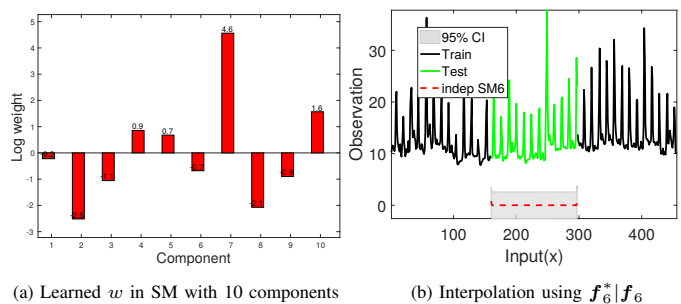


Fig. 4. Illustration of the learned w (a) in the SM and the interpolation result (b) of the 6-th SM component with a smaller weight. Here, the predictive amplitude of the 6-th SM component is almost zero and less important for the final predictive distribution and thus can be pruned.

We simply think that a component with a weight smaller than 1 is less important and has a small percentage of the full signal energy because the signal energy of data usually has exponential magnitude. Therefore, these components must contribute little to the underlying function. Furthermore, taking the sixth component as an example, we show its interpolation using $f_6^*|f_6$ in subplot (b) in Fig. 4. Interestingly, due to the small weight of the sixth component, the mean of its predictive distribution is very close to zero and far away from the testing value. Removing such components with small weights does not affect the learning and generalization ability of a GP model.

By keeping the rest of the important components with large weights, the SMD can reduce the parameter counts of the learned model, improve inference efficiency, and avoid overfitting without loss of performance. Consequently, we propose a pruning method to compress the SMD for the GP model. First, we identify important components by training a GP and pruning its components with the smallest weights. Second, we use the remaining unpruned components to constitute the structure of the compressed SMD. The pruning method is described in steps 18-28 of the **Algorithm 1**. Through this pruning strategy, we can reduce the number of hyper-parameters to $5Q_{rest}$. Here, we define a CR for the SMD, $\alpha_{CR} = \frac{Q_{rest}}{Q_{init}} \times 100\%$, to assess how much the SMD is compressed.

Remark 4: α_{CR} is an indicator of the pruning degree of the SMD using the SA algorithm. α_{CR} is zero if all components are pruned with $Q_{rest} = 0$ and 1 if all components are kept with $Q_{rest} = 1$.

C. Sparse dependency structure and behavior

In this section, we investigate the sparsity and behavior of the dependency structures between components. Observed from the definition of the SMD in Eq. (18), there are $Q^2 - Q$ dependency structures. In fact, we do not need an excessive amount of dependency structures because some dependency structures between components located far from each other are very weak. From Eq. (16), we can clearly observe that the closer the frequency μ_i , scale Σ_i and weight w_i between the components in SM are, the greater the dependency is in SMD, and vice versa. For two components located far from each other, the intersection between their SDs is infinitely close to zero, which means that their dependency structure is also very small. Therefore, we can confidently remove the low intensity dependency structures.

On the other hand, the sparsity of the dependency structures can be determined by its behavior. As shown in subplot (a) of Fig. 5, with w_i , σ_i^2 , w_j , and σ_j^2 of components i and j fixed, a_{ij} decays very fast with increasing of difference between μ_i and μ_j . This decaying behavior also tells us that the dependency of two components is approximately zero when the distance between their locations is large. Hence, based on a_{ij} , which determines the magnitude of the dependency structure, we can obtain an SMD kernel with sparse dependency by reducing the dependency structures with very small a_{ij} . Thus, we introduce a binary scalar β_{ij} in the SA algorithm to indicate the usage of the dependency between components i and j . The compressed SMD with sparse dependencies can be written as

$$k_{SMD}^{SA}(\boldsymbol{\tau}) = \sum_{i=1}^{Q_{rest}} \sum_{j=1}^{Q_{rest}} \beta_{ij} c_{ij} \exp(-2\pi^2 \boldsymbol{\tau}_\theta^\top \Sigma_{ij} \boldsymbol{\tau}_\theta) \times \cos\left(2\pi\left(\boldsymbol{\tau}_\theta^\top \boldsymbol{\mu}_{ij} - \frac{\phi_{ij}}{2}\right)\right), \quad (22)$$

where the superscript SA denotes the SA algorithm given before and $\beta_{ij} = 0$ if $c_{ij} < 1$ and $i \neq j$; otherwise, $\beta_{ij} = 1$.

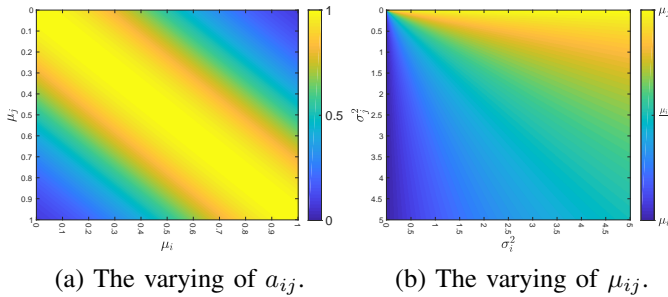


Fig. 5. Illustration of the varying of a_{ij} and μ_{ij} in the dependency structure of the SMD. In subplot (a), given σ_i^2 and σ_j^2 , a_{ij} decays very fast with increasing difference between μ_i and μ_j . In subplot (b), given μ_i and μ_j , a larger σ_i^2 will push μ_{ij} to the opposite position of μ_j .

Furthermore, we explore the features of the dependency structure in the SMD. Given μ_i and μ_j of components i and j

in SMD, we demonstrate the variations in μ_{ij} of the dependency between μ_i and μ_j in subplot (b) in Fig. 5. Interestingly, the mean position of the dependency tends to the side of the component with large variance. For components i and j , when σ_i^2 is equal to σ_j^2 , the μ_{ij} of their dependency is located at the midpoint between μ_i and μ_j . In addition, Fig. 1 shows the neat contribution of the dependency structure to the final kernel even with zero time and phase delay. When $\theta \neq 0$ or $\phi \neq 0$, the covariance of the dependency is shifted and centered at a different position. Here, we define an SR of the dependency for SMD, $\alpha_{SR} = \left(1 - \frac{\sum_{i=1}^{Q_{rest}} \sum_{j=1}^{Q_{rest}} \beta_{ij}}{Q_{rest}^2 - Q_{rest}}\right) \times 100\%$, to evaluate how sparse the SMD is.

Remark 5: The α_{SR} is ensured to be in the range of $[0, 1]$. α_{SR} is 1 if there is no significant dependency or 0 if there is full dependency.

VII. COMPARISONS BETWEEN THE SPECTRAL MIXTURE WITH DEPENDENCY STRUCTURE AND OTHER KERNELS

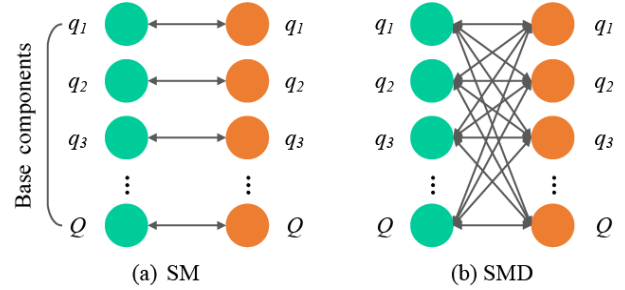


Fig. 6. SM kernel vs SMD kernel with Q components, where $q_i = \{1, \dots, Q\}$ denotes the i -th SM component. (a) The SM models only the auto-convolution between the basis component itself. (b) The SMD models both auto- and cross-convolution between the basis components.

Figure 6 visualizes the convolution differences between the SM and SMD, where each link (in black solid) represents a convolution structure of the kernel. Circle q_i corresponds to a GP f_i . The cross connection denotes a dependency of GPs f_i and f_j . Apparently, the SM considers only the auto-convolution of the basis component and ignores the dependency structures between components. Table I summarizes the differences between the SMD and SM kernels in terms of their hyper-parameters for a P -dimensional input setting. For NSM in this comparison, each hyper-parameter of the original SM is parameterized as a GP with a squared exponential (SE) kernel, for instance the weight w becomes $w_{i,\mathbf{x}} \sim \mathcal{GP}(0, k_{SE}(\mathbf{x}, \mathbf{x}'))$ in NSM. Thus NSM need three times hyper-parameter space than SM because the GP, $w_{i,\mathbf{x}}$, with a SE kernel usually has three hyper-parameters. When there is no incorporation of time and phase delay, the hyper-parameter space of the SMD is equal to that of the SM. The price paid for incorporating both the time and phase delay in the SMD is that the gradient computation for the SMD is more involved because additional time and phase delay hyper-parameters between basis components are introduced.

We now compare the SM and SMD on the same observations from a 1-dimensional input sampled from a $\mathcal{GP}(0, K_{SM} + K_{SMD})$, using the same values for both initial parameters and

TABLE I

COMPARISONS BETWEEN THE SMD AND OTHER SM KERNELS IN TERMS OF HYPER-PARAMETERS AND NUMBER OF HYPER-PARAMETERS. P IS THE DIMENSION OF INPUT. FOR AN INITIAL LARGE Q IN THE SM AND SMD, Q_{rest} IS MUCH SMALLER THAN Q AND $\alpha_{SR} > 0.5$.

| Kernel | Hyper-parameters | Number of hyper-parameters |
|---------------------------|--|-------------------------------------|
| SM | $\{w_i, \mu_i, \Sigma_i\}_{i=1}^Q$ | $(2P + 1)Q$ |
| NSM | $\{w_{i,x}, \mu_{i,x}, \Sigma_{i,x}\}_{i=1}^Q$ | $3 \times (2P + 1)Q$ |
| SMD $_{\phi=0, \theta=0}$ | $\{w_i, \mu_i, \Sigma_i\}_{i=1}^Q$ | $(2P + 1)Q$ |
| SMD | $\{w_i, \mu_i, \Sigma_i, \theta_i, \phi_i\}_{i=1}^Q$ | $(4P + 1)Q$ |
| Compressed SMD | $\{w_i, \mu_i, \Sigma_i, \theta_i, \phi_i\}_{i=1}^Q$ | $(4P + 1)Q_{rest}$ |
| SMD with SA | $\{w_i, \mu_i, \Sigma_i, \theta_i, \phi_i\}_{i=1}^Q$ | $(1 + 2P(2 - \alpha_{SR}))Q_{rest}$ |

noise (see Figure 1). Note that all plots of the SM and SMD covariance, SD, and function have the same output scale for comparison.

Remark 6: According to Eq. (18), Eq. (19), and Eq. (6), the covariances for diagonal elements of the trained kernel matrix (i.e., with $\tau = 0$) are:

- $k_{SM}(0) = \sum_{i=1}^Q w_i$
- $k_{SMD}(0, \theta = \mathbf{0}, \phi = \mathbf{0}) = \sum_{i=1}^{Q_{rest}} \sum_{j=1}^{Q_{rest}} \beta_{ij} c_{ij}$
- $k_{SMD}^{SA}(0) = \sum_{i=1}^{Q_{rest}} \sum_{j=1}^{Q_{rest}} \beta_{ij} c_{ij} \exp\left(-\frac{\pi^2}{2} \theta_{ij}^\top \Sigma_{ij} \theta_{ij}\right) \times \cos\left(-\pi(\theta_{ij} \mu_{ij} + \phi_{ij})\right)$
- $\gamma_{ij}(0) = a_{ij} \exp\left(-\frac{\pi^2}{2} \theta_{ij}^\top \Sigma_{ij} \theta_{ij}\right) \cos\left(\pi(\theta_{ij} \mu_{ij} + \phi_{ij})\right)$

Observe that while the diagonal values of the kernel matrix in the SM do not involve the hyper-parameters μ_i, Σ_i , for the SMD, the diagonal values are affected by all hyper-parameters including the time and phase delay.

From Figure 1, the differences, in terms of amplitude, peak, and trend between the covariance functions of the SM (dashed red) and SMD (dashed blue), are distinct. For the SMD, there are dependence structures (in cyan) that have the corresponding SD also modeled by a Gaussian distribution in the frequency domain, which contributes to an SM with a different magnitude. Without considering time and phase delays, subplots (d) and (e) of Figure 1 show that the dependency structure in SMD can reinforce the magnitudes of both SD and covariance in SM (shown in subplots (a) and (b)), but doesn't change the decaying behaviour of the covariance a lot. When incorporating both time and phase delays, the dependency structure determines whether SM components reinforce or weaken each other. Specifically, in subplots (g, h, j, k, m, and n), the dependency structure can largely change the magnitudes of both SD and covariance, shape of SD, and decaying behaviour of the covariance, and further reduce the predictive uncertainty. Given six observations (marked with black crosses) and conditions on them, we can obtain the learned posterior distribution and sampling path. Interestingly, regardless of whether the time and phase delay are considered, we can observe that the predictive CI of the SMD is significantly tighter (in blue shadow) than that of the SM (in red shadow).

VIII. EXPERIMENTS

In this section, we comprehensively investigate the performance of the SMD and compare it with that of state-of-the-art kernels on both synthetic and real-world datasets.

For all models, we run experiments 10 times and compute the mean and standard deviation of the 10 experimental results. For all experiments, the popular kernels implemented in the GPML toolbox [3] are used as baselines, such as the linear (LIN), SE, polynomial (Poly), periodic (PER), rational quadratic (RQ), Matérn (MA), Gabor, fractional Brownian motion covariance (FBM), underdamped linear Langevin process covariance (ULL), neural network (NN) and SM kernels. We also consider the recent non-stationary spectral mixture (NSM) kernel introduced in [11]. For each dataset, the same number of components Q is used for the SM, NSM and SMD. In all plots, the training, testing, SM predictions, SMD predictions, and CI are shown in black, green, red, blue, and gray shadows, respectively.

A. Dataset

The first experiment with synthetic data aims to illustrate the benefits of directly modeling phase and delay dependencies. Next, we compare the SMD with the original SM kernel for prediction tasks on multiple real-life datasets: monthly river flow and yearly sunspot. The first two experiments with real-life datasets comparatively illustrate the capability of GPs with the considered kernels to model irregular trends. The river flow and sunspot datasets are generated from an underlying natural phenomenon that involve limited or no human activity. They demonstrate complex dependencies in their patterns due to the physical interference in connection with the relative orbital position of solar planets.

B. Model assessment

In this paper, we apply multiple metrics to assess the performances and characteristics of different models.

- The mean-squared-error, $MSE \triangleq \frac{1}{n} \sum_{i=1}^n (y_i^* - \tilde{y}_i^*)^2$, is employed to measure the generalization performance of the GP models.
- The 95% CI (instead of, e.g., error bar) is used to visualize the uncertainty (see Eq. (3)) of the output.
- In addition to these performance metrics, we consider the posterior correlation ρ_{ij} (see Eq. (11)) to quantify the latent dependency between the SM components.
- The learned dependency γ_{ij} (see Eq. (20)) of the SMD variant with the best MSE performance is used to demonstrate the underlying dependency between the SM components and dependency structure learned by the SMD.
- We exhibit the CR and SR of the SMD by computing α_{CR} and α_{SR} , respectively.

With the above metrics, the results shown in this section should be sufficient to support the superiority of the SMD. Due to page limitations, additional experimental results and discussions are presented in the supplement.

C. Learning a synthetic signal with dependency structures

We illustrate the capability of the SMD to capture time and phase delay dependencies using an artificial dataset. The dataset is sampled from the following GP with a hybrid kernel structure

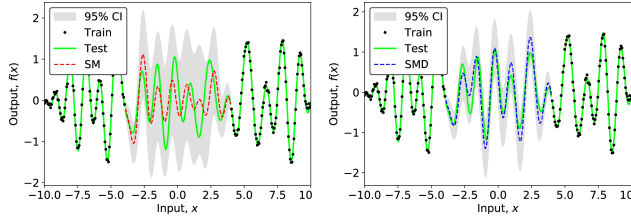


Fig. 7. Performance of the SM (left) and SMD (right) on a synthetic signal. The testing data are the middle part (40%) of the signal.

consisting of the sum of an SMD with dependent structures and an SM with independent structures, both kernels with $Q = 2$ components: $f(x) \sim \mathcal{GP}(0, k_{SMD}(\theta_i = \{0.1, 0.3\}_{i=1}^2, \phi_i = \{0.1, 0.3\}_{i=1}^2) + k_{SM})$. We generate a normal time series of length 300 in the interval $[-10, 10]$ and add some noise to it (see Figure 7). In this experiment, we remove the middle 40% of the signal and consider it as missing testing data (in green). The rest of the signal forms the training data (in black). Both SMD and SM are configured with the same number of components $Q = 5$ for all experiments and with the same initial values for the hyper-parameters w_i, μ_i, σ_i^2 . The other parameters of k_{SMD}, θ_i and ϕ_i , are initialized randomly.

The difference in the performance of SMD and SM is clear in terms of fitting and uncertainty quantification. The SMD is capable of learning the hybrid covariance structure well. For the SM (dashed red), it is more difficult to recognize such dependent structures and to interpolate the missing block. Obviously, the SMD yields better prediction and smoother CIs than the SM (see Figure 7). Overall, this experiment indicates the capability of the SMD to correctly capture dependent patterns of the generative signal and achieve the lowest MSE. (see Table II). As a result of simultaneously introducing time and phase delay in the kernel of the synthetic signal, here, the SMD without time and phase delays, only time delay, or only phase delay is unable to extrapolate the missing block well.

D. Long range interpolation of monthly river flow

As is well known, interpolation is a general purpose for GP-related tasks. In this experiment, we validate long range interpolation abilities using GPs with SMD. Here, we consider the monthly river flow dataset revealing patterns related to time and phase with variability over the period of recording. In particular, the moon and sun are primarily responsible for the rising and falling of river tidal flows, and such effects are delayed and augmented by gravity and resonances. The mean monthly river flow in the Madison River near West Yellowstone is the average flow from 1923 to 1960 [31]. Empirical analysis [31] shows various characteristics of this flow data experiment: short term monthly variations, medium term seasonal patterns and nonstrict periodic long term trends related to the relative positions of the moon and sun and some white noise.

As such, the monthly river flow involves limited influence from human activity and contains complicated patterns (see Figure 8). There are multiple short term, medium-term and long term trends containing time and phase delays in the monthly river flow time series because the appearance time of the flow peak is not periodical and its amplitude is always irregular.

There are 456 values in the time series. Here, 30% of the data, namely, the long range middle part, is removed for testing, while the rest of the data are used for training. We initially use $Q = 20$ components. Hyper-parameters μ, Σ are initialized through **Algorithm 2** for both the SMD and SM, while θ and ϕ are randomly initialized for k_{SMD} .

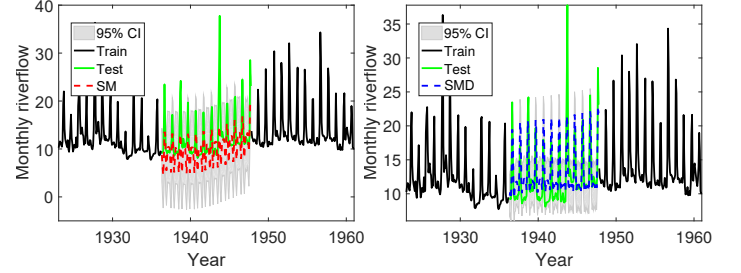


Fig. 8. Performance of a GP with the SM kernel (left) versus the SMD (right) kernel on the monthly river flow dataset.

The results indicate that both the SMD and SM can interpolate the missing month river flow well. However, the SMD achieves better performance and confidence. Apparently, the SMD is in general more effective in modeling complex patterns hidden in these data (see Table II and Figure 8). Using the same initial number of components Q and the SA algorithm, Table III shows that SMD achieves a better CR of 38.9%. Particularly, in this case, the SR of 89.3% indicates that most of the dependency structures in the SMD are removed due to low intensity.

E. Joint interpolation and extrapolation of yearly sunspots

In addition to interpolation, in this experiment, we simultaneously perform interpolation and extrapolation to further substantiate the learning ability of the SMD. We consider the yearly sunspot number dataset¹ collected between 1700 and 2014. The historical evolution of yearly sunspots can help explain spatial magnetic field environment changes affected by the sun activities. The yearly sunspot number is obtained by taking a simple arithmetic mean of the daily total sunspot number over all days of each year. Sunspots appear as spots darker than the surrounding areas on the sun's photosphere [32]. They usually have lower surface temperatures than the areas around them. A sunspot has an unstable period of existence: the average number of sunspots that is monitored increases and decreases with a quasiperiod. There are dependencies between patterns of sunspots caused by some physical types of interference. This is another example of data generated by a natural process involving limited human activity. As shown in Figure 9, patterns in yearly sunspots contain various irregular peaks over 315 years. The peak values indicate large variations.

There are 315 records in the time series. We use the last 10% of the data for extrapolation (in solid green) in the testing dataset and randomly sample 20% of the original data from the first 90% of the yearly sunspots as the interpolation testing (in crossed green) dataset. The remaining 70% of the data are used for training (in black). The legends Test_{ext} and Test_{int} denote

¹<http://www.sidc.be/silso/infosnotyearly>

the testing data of extrapolation and interpolation, respectively. Note that the training data are not equally sampled due to the presence of missing values to be interpolated. Therefore, hyper-parameter initialization is not effective because the FT does not favor the unequally sampled training data. Time and phase delays in the SMD are also randomly initialized. We initially consider $Q = 20$ components for both SMD and SM.

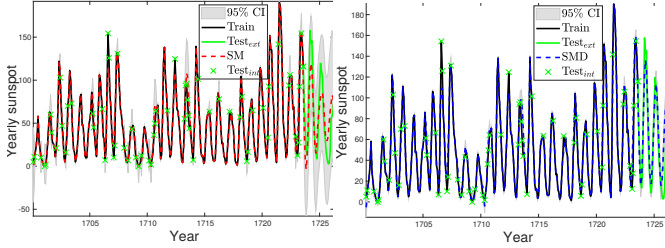


Fig. 9. Performance of a GP with the SM (left) and SMD (right) kernels on the yearly sunspot dataset.

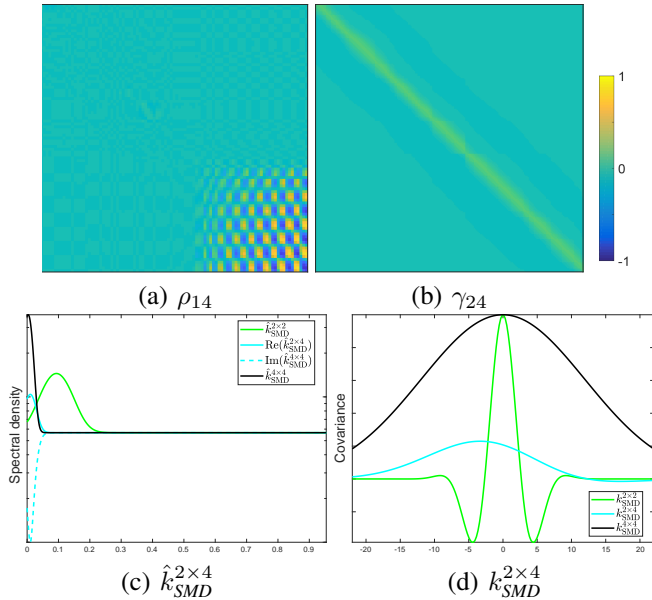


Fig. 10. The dependency structures on the yearly sunspot dataset. Subplot (a): the posterior correlations ρ_{14} of the SM kernel. Subplot (b): the learned dependencies γ_{24} of the SMD kernel. Subplot (c): the SDs of $k_{SMD}^{2 \times 2}$, real part $\text{Re}(k_{SMD}^{2 \times 4})$, imaginary part $\text{Im}(k_{SMD}^{2 \times 4})$, and $k_{SMD}^{4 \times 4}$ are in green, solid cyan, dashed cyan, and black, respectively. Subplot (d): the covariances of $k_{SMD}^{2 \times 2}$, $k_{SMD}^{2 \times 4}$, and $k_{SMD}^{4 \times 4}$ are in green, cyan, and black, respectively.

Subplot (a) of Fig. 10 shows high and complex posterior correlation coefficient values ρ_{14} in the SM. In subplot (b), we present the learned dependencies between the components in the SMD, as indicated by the positive and negative values of γ_{24} . From subplots (c) and (d), there are significant time and phase delay dependency structure (in cyan) between components 2 (in green) and 4 (in black) in the SMD. As investigated in Section VI-C, the mean position of $k_{SMD}^{2 \times 4}$ is close to component 4 because component 2 has a larger variance. Due to the time and phase delay, the covariance of $k_{SMD}^{2 \times 4}$ is shifted. The period of the dependency structure $k_{SMD}^{2 \times 4}$ is smaller than the 2nd component and larger than the 4th component and corresponds to the location of $k_{SMD}^{2 \times 4}$. From the CR and SR shown in

Table III, the SMD using the SA algorithm can reduce the hyper-parameter size by 40.7% and dependency structures by 50.3%. The above results indicate that both the SMD and SM are able to interpolate missing values well with a small CI. However, for the extrapolation task, the SMD achieves better performance and confidence (see Table II and Figure 9). With this experimental result, we can conclude that the SMD can perform interpolation and extrapolation equally well for incomplete signals.

F. Discussion

TABLE II
PERFORMANCES OF VARIOUS BASELINES VERSUS THE SMD IN TERMS OF MSE. HERE, RI AND BI DENOTE RANDOM INITIALIZATION (RI) AND BOOTSTRAP-BASED INITIALIZATION (BI) OF HYPER-PARAMETERS, RESPECTIVELY.

| Kernel | Synthetic | Riverflow | Sunspot |
|---|--------------------|--------------------|-----------------------|
| LIN | 0.32 ± 0.11 | 24.37 ± 4.57 | 1617.45 ± 131.63 |
| SE | 0.31 ± 0.20 | 174.14 ± 19.23 | 591.24 ± 9.21 |
| Poly | 0.32 ± 0.18 | 182.01 ± 18.73 | 1627.02 ± 127.84 |
| PER | 0.35 ± 0.13 | 20.31 ± 7.22 | 1533.84 ± 143.15 |
| RQ | 0.31 ± 0.10 | 24.88 ± 6.32 | 307.22 ± 30.38 |
| MA | 0.32 ± 0.14 | 170.29 ± 18.90 | 590.72 ± 26.21 |
| Gabor | 0.31 ± 0.20 | 22.51 ± 3.37 | 4047.83 ± 19.78 |
| FBM | 0.49 ± 0.19 | 23.84 ± 3.21 | 6428.69 ± 515.98 |
| ULL | 0.26 ± 0.11 | 168.06 ± 18.16 | 467.08 ± 23.90 |
| NN | 0.32 ± 0.16 | 23.65 ± 2.32 | 1522.67 ± 68.58 |
| NSM | 0.53 ± 0.21 | 166.85 ± 20.45 | 4697.24 ± 375.15 |
| SM (RI) | 0.41 ± 0.16 | 23.55 ± 2.79 | 363.64 ± 64.32 |
| SM (BI) | 0.43 ± 0.18 | 13.91 ± 1.78 | 270.78 ± 13.96 |
| SMD (RI, $\theta = 0, \phi = 0$) | 0.47 ± 0.13 | 23.31 ± 4.76 | 329.81 ± 18.19 |
| SMD (BI, $\theta = 0, \phi = 0$) | 0.28 ± 0.14 | 9.55 ± 1.79 | 184.47 ± 18.58 |
| SMD (RI, $\theta \neq 0, \phi \neq 0$) | 0.45 ± 0.95 | 19.26 ± 3.53 | 322.50 ± 21.67 |
| SMD (BI, $\theta \neq 0, \phi \neq 0$) | 0.05 ± 0.01 | 8.96 ± 0.72 | 171.16 ± 13.10 |

On the riverflow and sunspot datasets, the results shown in Table II demonstrate that the SMD ($\theta \neq 0, \phi \neq 0$) performs better than the other SMD variants ($\theta = 0$ or $\phi = 0$). These datasets consist of recorded measurements from natural phenomena with possible dependency between patterns. They contain physical patterns involving some form of interference. For instance, in the monthly river flow extrapolation task, the moon and sun are primarily responsible for the rising and falling of river tidal flows, which are delayed and augmented under the influence of gravity and resonances. The results of experiments on these datasets show the benefits of the SMD variant with $\theta \neq 0, \phi \neq 0$ to improve performance when modeling natural phenomena with very limited human intervention.

On these datasets, the performance of the SMD with $\theta \neq 0$ and $\phi \neq 0$ is better than that of the other SMD variants ($\theta = 0$ or $\phi = 0$; see Table II). In particular, the SM and SMDs using BI exhibit much better performance than those using random initialization (RI). Clearly, the proposed BI in the SA algorithm is capable of providing a good starting point for optimization in high-dimensional hyper-parameter space.

As shown in Table III, the CRs of both the SM and SMD are larger than 30% due to the use of the SA algorithm. In other words, by using the SA algorithm, a considerable proportion of the number of components used in the SMD and SM can be pruned to reduce the hyper-parameter space. In Table III,

TABLE III
THE AVERAGE CRS AND SRs OF THE SM AND SMD VARIANTS USING SA.

| Kernel | CR | CR | SR | SR |
|--|--------------|--------------|--------------|---------|
| | Riverflow | Sunspot | Riverflow | Sunspot |
| SM | 33.2% | 30.3% | – | – |
| SMD ($\theta = \mathbf{0}, \phi = \mathbf{0}$) | 35.3% | 32.8% | 89.1% | 57.6% |
| SMD ($\theta \neq \mathbf{0}, \phi \neq \mathbf{0}$) | 38.9% | 40.7% | 89.3% | 55.3% |

we observe that the SMDs with SA usually have better CR than the SM. This may be caused by the fact that the SMD has a better representation ability than the SM. The SMD can describe an underlying function with fewer components than the SM because the latter needs additional components to delineate the latent dependency structure. In addition, Table III shows that the SR of all the SMDs is high, which means that the dependency structures exhibit substantial sparsity. Most dependency structures are very small and removable. Due to the higher number of hyper-parameters of the NSM (at least three times the number of hyper-parameters of the SM), the results in Table II show unsatisfactory performance from the NSM on the synthetic dataset containing dependent structures, as well as on real-world datasets (note that the NSM is not applicable for non-Cartesian multidimensional, i.e. $P > 2$, datasets). Thus, on small datasets, NSM is troubled by overfitting.

IX. CONCLUSION

We propose a novel SMD kernel, which extends the SM kernel by incorporating time and phase delay dependency structures between the basis kernel components. An interpretable SA algorithm for the SMD is introduced to initialize its hyper-parameters, to automatically compress basis components and obtain sparse dependency structures.

The results of extensive experiments on both the synthetic and real-life datasets indicate that the SMD using the structure adaptation (SA) algorithm is capable of capturing time and phase delay dependency structures between basis kernel components. Experimental results also have shown that the SMD can identify and model the structure involved in the data and perform accurate forecasting of long-term trends. The benefits of the SMD are shown to be more evident when modeling natural phenomena with very limited or no human intervention.

REFERENCES

[1] S. Theodoridis, *Machine learning: a Bayesian and optimization perspective, 2nd edition.* Academic press, 2020.
 [2] C. E. Rasmussen and H. Nickisch, “Gaussian processes for machine learning (gpml) toolbox,” *Journal of Machine Learning Research*, vol. 11, no. Nov, pp. 3011–3015, 2010.
 [3] C. E. Rasmussen and C. K. Williams, *Gaussian process for machine learning.* MIT press, 2006.
 [4] F. Yin and F. Gunnarsson, “Distributed recursive Gaussian processes for rss map applied to target tracking,” *IEEE Journal of Selected Topics in Signal Processing*, vol. 11, no. 3, pp. 492–503, 2017.
 [5] Y. Xu, F. Yin, W. Xu, J. Lin, and S. Cui, “Wireless traffic prediction with scalable Gaussian process: Framework, algorithms, and verification,” *IEEE J. Sel. Areas Commun.*, vol. 37, no. 6, pp. 1291–1306, Jun. 2019.
 [6] F. Yin, Z. Lin, Q. Kong, Y. Xu, D. Li, S. Theodoridis, and S. R. Cui, “Fedloc: Federated learning framework for data-driven cooperative localization and location data processing,” *IEEE Open Journal of Signal Processing*, vol. 1, pp. 187–215, 2020.

[7] A. Wilson and R. Adams, “Gaussian process kernels for pattern discovery and extrapolation,” in *Proceedings of the 30th International Conference on Machine Learning (ICML-13)*, 2013, pp. 1067–1075.
 [8] D. Duvenaud, J. R. Lloyd, R. Grosse, J. B. Tenenbaum, and Z. Ghahramani, “Structure discovery in nonparametric regression through compositional kernel search,” *arXiv preprint arXiv:1302.4922*, 2013.
 [9] F. Yin, L. Pan, T. Chen, S. Theodoridis, Z.-Q. T. Luo, and A. M. Zoubir, “Linear multiple low-rank kernel based stationary Gaussian processes regression for time series,” *IEEE Transactions on Signal Processing*, vol. 68, pp. 5260–5275, 2020.
 [10] Y. Dai, T. Zhang, Z. Lin, F. Yin, S. Theodoridis, and S. Cui, “An interpretable and sample efficient deep kernel for Gaussian process,” in *Conference on Uncertainty in Artificial Intelligence.* PMLR, 2020, pp. 759–768.
 [11] S. Remes, M. Heinonen, and S. Kaski, “Non-stationary spectral kernels,” in *Advances in Neural Information Processing Systems*, 2017, pp. 4645–4654.
 [12] A. G. Wilson, E. Gilboa, A. Nehorai, and J. P. Cunningham, “Fast kernel learning for multidimensional pattern extrapolation,” in *Advances in Neural Information Processing Systems*, 2014, pp. 3626–3634.
 [13] K. R. Ulrich, D. E. Carlson, K. Dzirasa, and L. Carin, “GP kernels for cross-spectrum analysis,” in *Advances in neural information processing systems*, 2015, pp. 1999–2007.
 [14] G. Parra and F. Tobar, “Spectral mixture kernels for multi-output Gaussian processes,” in *Advances in Neural Information Processing Systems 2017, Long Beach, CA, USA, 2017*, pp. 6684–6693.
 [15] R. Dürichen, M. A. Pimentel, L. Clifton, A. Schweikard, and D. A. Clifton, “Multitask Gaussian processes for multivariate physiological time-series analysis,” *IEEE Transactions on Biomedical Engineering*, vol. 62, no. 1, pp. 314–322, 2015.
 [16] M. Kupilik, F. Witmer, E.-A. MacLeod, C. Wang, and T. Ravens, “Gaussian process regression for arctic coastal erosion forecasting,” *arXiv preprint arXiv:1712.00867*, 2017.
 [17] K. Chen, T. van Laarhoven, P. Groot, J. Chen, and E. Marchiori, “Multioutput convolution spectral mixture for Gaussian processes,” *IEEE Transactions on Neural Networks and Learning Systems*, 2019.
 [18] K. Chen, T. van Laarhoven, J. Chen, and E. Marchiori, “Incorporating dependencies in spectral kernels for Gaussian processes,” in *Machine Learning and Knowledge Discovery in Databases - European Conference, ECML PKDD 2019, Würzburg, Germany, 2019, Proceedings*, 2019.
 [19] S. Bochner, *Lectures on Fourier Integrals.(AM-42).* Princeton University Press, 2016, vol. 42.
 [20] M. L. Stein, *Interpolation of spatial data: some theory for Kriging.* Springer Science & Business Media, 2012.
 [21] D. Duvenaud, “Automatic model construction with Gaussian processes,” Ph.D. dissertation, University of Cambridge, 2014.
 [22] Y.-L. K. Samo and S. Roberts, “Generalized spectral kernels,” *arXiv preprint arXiv:1506.02236*, 2015.
 [23] W. Herlands, A. Wilson, H. Nickisch, S. Flaxman, D. Neill, W. Van Panhuis, and E. Xing, “Scalable Gaussian processes for characterizing multidimensional change surfaces,” in *Artificial Intelligence and Statistics*, 2016, pp. 1013–1021.
 [24] P. A. Jang, A. Loeb, M. Davidow, and A. G. Wilson, “Scalable Lévy process priors for spectral kernel learning,” in *Advances in Neural Information Processing Systems*, 2017, pp. 3943–3952.
 [25] Bernard, *Theory and application of digital signal processing.* Prentice-Hall, 1975.
 [26] H. Bateman, *Tables of integral transforms [volumes I & II].* McGraw-Hill Book Company, 1954, vol. 1.
 [27] G. Gaspari and S. E. Cohn, “Construction of correlation functions in two and three dimensions,” *Quarterly Journal of the Royal Meteorological Society*, vol. 125, no. 554, pp. 723–757, 1999.
 [28] M. G. Genton, W. Kleiber *et al.*, “Cross-covariance functions for multivariate geostatistics,” *Statistical Science*, vol. 30, no. 2, pp. 147–163, 2015.
 [29] A. M. Zoubir and B. Boashash, “The Bootstrap and its application in signal processing,” *IEEE signal processing magazine*, vol. 15, no. 1, pp. 56–76, 1998.
 [30] L. Scrucca, M. Fop, T. B. Murphy, and A. E. Raftery, “mclust 5: clustering, classification and density estimation using Gaussian finite mixture models,” *The R journal*, vol. 8, no. 1, p. 289, 2016.
 [31] K. W. Hipel and A. I. McLeod, *Time series modelling of water resources and environmental systems.* Elsevier, 1994, vol. 45.
 [32] R. C. Willson, S. Gulkis, M. Janssen, H. S. Hudson, and G. A. Chapman, “Observations of solar irradiance variability,” *Science*, vol. 211, no. 4483, pp. 700–702, 1981.